FAST PSF SYNTHESIS WITH DEFOCUSED AND SPHERICAL ABERRATION

Nicholas Ganino and Qi Guo

Elmore Family School of Electrical and Computer Engineering
Purdue University

ABSTRACT

Accurately estimating the point spread function (PSF) of an optical system requires solving free-space wave propagation, which entails evaluating a diffraction integral. This integral is traditionally computed numerically using FFT or Hankel transforms, as it lacks a closed-form solution. We show that, under defocus and spherical aberration, the diffraction integral admits an approximate closed-form solution by combining a piecewise Bessel approximation with Gaussian-type integrals. Based on this result, we develop a fast wave-based PSF simulator with linear complexity in the radial resolution. The proposed, un-optimized simulator achieves up to a 2× speedup over Hankel-based integration and a 4× speedup over FFT while closely matching wave-optical PSFs, enabling efficient large-scale depth-of-field synthesis.

***Index Terms*—** point spread function, defocus, aberration, Bessel function

1. INTRODUCTION

Efficient and accurate synthesis of depth-of-field (DoF) images is critical for a wide range of computer vision and graphics applications, including depth from defocus [1, 2, 3], image restoration [4, 5, 6], and rendering [7, 8]. Despite its importance, DoF synthesis remains challenging because it requires evaluating point spread functions (PSFs) at a densely sampled set of image locations. Geometric PSF simulators [1] are computationally efficient, but they fail to capture diffraction effects and often suffer from discretization artifacts, especially near focus (Fig. 1). In contrast, wave-based PSF simulators [9] provide high physical accuracy but incur substantial computational cost due to the numerical evaluation of diffraction integrals. These limitations motivate the need for a PSF simulator that is both fast and accurate, enabling practical DoF image synthesis at scale.

This paper proposes a fast simulator that approximates the diffraction integral under defocus and spherical aberration in closed form. By avoiding expensive numerical integration, the proposed approach substantially reduces runtime while retaining diffraction effects, compared to wave-based simulators commonly used in recent work [10, 11, 12]. As shown in Fig. 1, our method produces visually accurate DoF images with a clear computational advantage over existing wave-based approaches, while also achieving higher accuracy than geometric simulation.

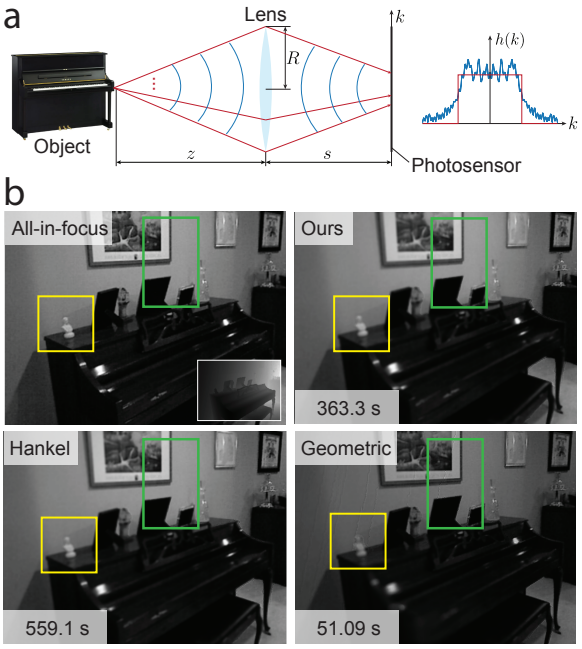

Fig. 1: Overview. (a) Wave-based (blue) and geometric-based (red) PSF synthesis. Wave-based simulation accurately models diffraction at high computational cost, while geometric simulation is fast but inaccurate. (b) DoF rendering via per-pixel PSF synthesis according to the provided depth map (inset). Our simulator achieves substantially lower runtime than the Hankel-based wave simulator used in recent work [10], while keeping high fidelity. Boxes highlight discretization artifacts in geometric rendering.

Existing wave-based methods follow the classic approach of Goodman [13], which typically evaluate the diffraction integral numerically using the Fast Fourier Transform (FFT). When the wavefront is radially symmetric, this evaluation can be reduced from two dimensions to one dimension and solved via the Hankel transform. Further simplification, however, is challenging due to the lack of closed-form solutions for diffraction integrals with general wavefront phase pro-

files. There have been work that combines geometric optics and wave optics to efficiently model aberrations in optical assemblies [14, 15]. However, these models still require solving diffraction integral within frameworks. People have also trained neural networks to implicitly represent the PSFs as a function of depth, incident angle, etc., but training these models still require data generated from solving diffraction integrals [16, 17, 18]. In this work, we directly tackle the simplification of the diffraction integral, which we haven't seen in prior works. We show that when the wavefront is parameterized by Seidel coefficients consisting only of defocus and spherical aberration, the diffraction integral admits an accurate approximate closed-form solution.

We derive this solution in detail, implement a fast PSF simulator based on it, and analyze its computational efficiency and accuracy relative to widely used FFT- and Hankel-based simulators. Experimental results demonstrate a $2\times$ speedup over Hankel-based methods and a $4\times$ speedup over FFT-based methods, while maintaining high fidelity in the synthesized PSF shapes. The proposed simulator is complementary to existing FFT- and Hankel-based approaches, trading generality for a significant gain in computational efficiency.

The main contributions of this paper are:

- An approximate closed-form solution to the diffraction integral under defocus and spherical aberration;
- A fast PSF simulator based on this solution;
- A comprehensive comparison with existing PSF simulation methods in terms of accuracy and runtime.

2. PRINCIPLE

Consider an on-axis point source located at distance z from a single-lens camera, emitting a spherical wavefront with wavelength λ, as illustrated in Fig. 1a. The lens is assumed to transmit all incident light within a circular aperture of radius R. Under these assumptions, the resulting point spread function (PSF) h on the photosensor is radially symmetric and can be expressed via the well-known Hankel transform

$$h(k) = \left| 2\pi \int_0^R P(r) J_0(2\pi k r)\, r\, dr \right|^2 . \tag{1}$$

The variables r and k denote the radial coordinate at the aperture and sensor plane, respectively, $J_0(\cdot)$ is the zeroth-order Bessel function of the first kind, and the pupil function $P(r)$ is given by:

$$P(r) = \exp\left(j2C_d\, r^2/R^2\right), \tag{2}$$

where C_d is the defocus coefficient:

$$C_d = \frac{\pi}{2\lambda}\left(z^{-1} + s^{-1} - f^{-1}\right).$$

Evaluating (1) typically requires either direct numerical integration, which can be formulated as a matrix multiplication with $O(N^2)$ complexity, or a Fast Hankel Transform (FHT) with $O(N \log N)$ complexity [19], where N denotes the number of radial samples of the PSF.

The key contribution of this work is an analytic approximation of the Bessel function $J_0(a)$ that enables a closed-form evaluation of the Hankel integral. Specifically, we adopt the following piecewise approximation:

$$\tilde{J}_0(a) = \begin{cases} f(a), & a \le 1, \\ g(a), & \text{otherwise}, \end{cases} \tag{3}$$

where

$$f(a) = 1 - \frac{a^2}{4} + \frac{a^4}{64},$$
$$g(a) = \sqrt{\frac{2}{\pi}}\left(\frac{3}{2}\alpha^{-\frac{1}{2}} - \pi k r\, \alpha^{-\frac{3}{2}} + \frac{1}{a}\right)\cos\left(a - \tfrac{\pi}{4}\right).$$

Here, α is a tunable hyperparameter that controls the accuracy of the asymptotic approximation. As shown in Fig. 2a, the proposed approximation $\tilde{J}_0(a)$ closely matches the true Bessel function $J_0(a)$ over the entire domain for representative values of the variable a.

Substituting $\tilde{J}_0$ into (1) yields a decomposition of the PSF into two integrals,

$$h(k) \approx 4\pi^2 \left| \int_0^{\frac{1}{2\pi k}} f(2\pi k r)\, \exp\left(j2C_d\, r^2\right) r\, dr + \int_{\frac{1}{2\pi k}}^{R} g(2\pi k r)\, \exp\left(j2C_d\, r^2\right) r\, dr \right|^2 . \tag{4}$$

Both integrals admit closed-form solutions by reducing to Gaussian-type integrals of the form [20]

$$\int \exp\left[-(\nu x^2 + 2\gamma x + \epsilon)\right] dx = \frac{1}{2}\sqrt{\frac{\pi}{\nu}} \exp\left(\frac{\gamma^2 - \nu\epsilon}{\nu}\right) \operatorname{erf}\left(\sqrt{\nu}\, x + \frac{\gamma}{\sqrt{\nu}}\right) + \text{constant}. \tag{5}$$

As a result, the PSF can be evaluated analytically with only $O(N)$ computational complexity, representing a substantial reduction compared to existing numerical and FHT-based approaches. For brevity, we omit the explicit closed-form expression in the main text and refer the reader to the Appendix for the full derivation.

Extension to Spherical Aberration. When both defocus and spherical aberrations are present, the pupil function can be written as

$$P(r) = \exp\left[j\left(\frac{2C_d r^2}{R^2} + \frac{C_s r^4}{R^4}\right)\right], \tag{6}$$

where C_s denotes the spherical aberration coefficient. The presence of the quartic term r^4 in the phase prevents the reduction of the Hankel integral to closed form using the previous approach.

To address this difficulty, we approximate the pupil function using a piecewise quadratic phase model. Specifically, we partition the pupil into M radial intervals $[r_i, r_{i+1})$, within each of which the phase is locally approximated by a quadratic function:

$$\tilde{P}(r) = \begin{cases} \exp\left[j\alpha_1 r^2\right], & 0 \le r < r_1, \\ \exp\left[j\alpha_2 r^2\right], & r_1 \le r < r_2, \\ \vdots & \\ \exp\left[j\alpha_M r^2\right], & r_{M-1} \le r < r_M, \end{cases} \tag{7}$$

where the coefficients $\{\alpha_i, \beta_i\}$ are chosen to best approximate the original quartic phase within each interval. As illustrated in Fig. 2b, the resulting piecewise approximation closely resembles the true pupil function.

With this approximation, each segment reduces to the same form as the purely defocus case in Eq. 4, allowing the PSF contribution of each interval to be evaluated analytically using Gaussian integrals. The overall PSF is then obtained by summing the contributions across all segments.

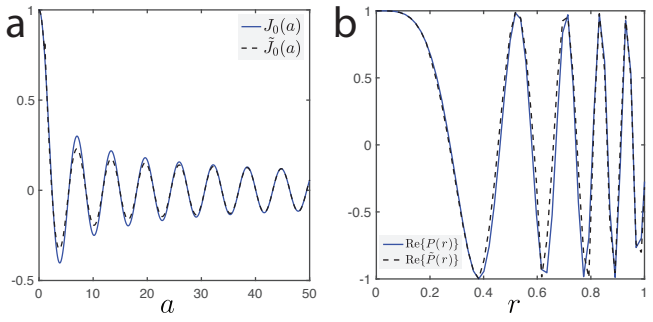

Fig. 2: (a) Zeroth-order Bessel function of the first kind $J_0(a)$ and its approximation $\tilde{J}_0(a)$. (b) Pupil function $P(r)$ and its approximation $\tilde{P}(r)$ with $C_d = 10$ and $C_s = 10$. Both approximations closely match their corresponding ground-truth functions.

3. RESULTS

This section analyzes the speed and accuracy trade-off of the proposed closed-form solution of defocused and spherical-aberrated PSFs. We chose the following methods as baselines, which have been frequently used in recent computational imaging works [9, 10, 1]. First, we evaluate of Hankel transform (Eq. 1) via matrix multiplication and then interpolate the radial PSF $h(k)$ to the two-dimensional PSF $h(\mathbf{x})$:

$$h(\mathbf{x}) \equiv h(k = \|\mathbf{x}\|). \tag{8}$$

We did not utilize FHT, as the disk pupil function violates the smoothness constraint that FHT requires and the calculated PSF significantly deviates from the plain Hankel transform. We implemented Hankel transform in Python scripts. Second, we directly calculate the 2D PSFs according to:

$$h(\mathbf{x}) \propto \left|\mathcal{F}\left[(\|\mathbf{x}\| < R) P(\|\mathbf{x}\|)\right]\right|^2. \tag{9}$$

via Fast Fourier Transform (FFT) by calling Scipy's fft function. Third, we use the simple geometric optics, where the PSF is a scaling of the pupil under the thin-lens model [1]:

$$h(\mathbf{x}) = \frac{1}{\sigma^2}\left(\frac{\|\mathbf{x}\|}{\sigma} < 1\right), \text{where } \sigma = Rs\left(\frac{1}{z} - \frac{1}{z_f}\right), \tag{10}$$

where s and z_f is the sensor and focal distance, and z is the target distance as in Fig. 1a. The defocus parameter C_d can be similarly calculated as [21]:

$$C_d = \frac{\pi(z_f - z)R}{8\lambda}\left(\frac{1}{s} + \frac{1}{z_f}\right). \tag{11}$$

For simplicity, we refer to these baseline PSF evaluation methods as *Hankel*, *FFT*, and *Geometric*. Hankel and FFT are wave-based, thus their outputs are consistent with each other, and can accurately render the diffraction effects in the PSFs, while Geometric cannot. We consider the output from Hankel and FFT to be the true PSFs in our evaluation. For our method, we compute the radial PSF $h(k)$ using the closed-form solution implemented in Python scripts and then interpolate it to 2D, similar to Hankel.

Range of realistic C_d and C_s. For the defocus parameter C_d, we set it to be smaller than 10 as larger PSFs will likely blur out textures in images. We surveyed stock lenses sold by major optical elements suppliers, and found that the spherical parameter C_s of typical lenses ranges from 0 to 10.

Time and accuracy. Fig. 3 compares runtime and accuracy among Hankel, FFT, and the proposed approach (ours). We exclude Geometric, as it is not a wave-based PSF simulator. The proposed method achieves a clear reduction in computational cost relative to the baselines while accurately reproducing defocus and spherical aberration effects. Fig. 4 further presents representative radial cross-sections of PSFs synthesized by different methods, demonstrating close qualitative agreement between our results and those of prior wave-based simulators when C_s is small. The experiment is conducted on a machine with an Intel Core i7-11370H 3.30GHz, Quad-Core Processor and a 32GB RAM.

Depth-of-field (DoF) rendering. Fig. 5 demonstrates a potential use case of the proposed PSF simulator. To accurately render the DoF effect in an image, we need to densely synthesize the PSFs of the scene. Our method's speed advantage leads to faster rendering than Hankel or FFT (Fig. 5b-e). Although Geometric can lead to even faster rendering, the

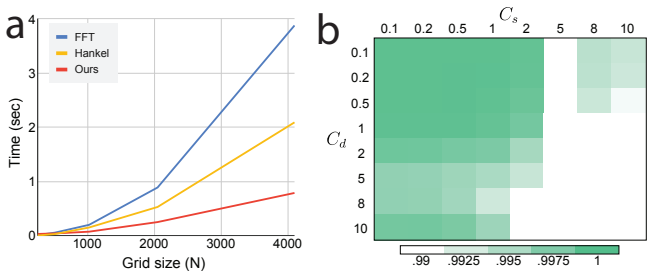

Fig. 3: Quantitative comparison of PSF synthesis runtime and accuracy. (a) Runtime for generating a 2D PSF across varying spatial resolutions N. Our method is consistently 2× faster than Hankel-based integration and 4× faster than FFT-based synthesis. (b) Cross-correlation coefficients between our approximation and the FFT-based simulation. Our simulated PSF achieves high accuracy when the spherical aberration coefficient C_s is less than 2.

rendered image suffer from discretization artifacts when the target texture is close to focus, as shown in Fig. 5f.

4. DISCUSSION

The proposed approximate closed-form PSF evaluation is complementary to the classic Hankel or FFT-based PSF evaluation. Ours clearly show the advantage in computational time, but it can only handle defocus and spherical aberrations at the current stage, while the latters are suitable for rendering PSFs for custom pupil functions. Because of this, ours is more suitable for synthesizing large scale, realistic DoF images for depth from defocus, image deblurring, etc., while the classic Hankel or FFT-based PSF simulators are for end-to-end design of computational imaging systems.

5. APPENDIX

Full derivation of the closed-form solution. Eq. 4 can be decomposed into the weighted summation of the following six forms of integrals:

$$
\begin{aligned}
h_1(k) &\triangleq \int_0^{a_0(k)} r\,\Phi(r)\,dr,\\
h_2(k) &\triangleq \int_0^{a_0(k)} r^3\,\Phi(r)\,dr,\\
h_3(k) &\triangleq \int_0^{a_0(k)} r^5\,\Phi(r)\,dr,\\
h_4(k) &\triangleq \int_{a_0(k)}^{R} C(r,k)\,\Phi(r;k)\,dr,\\
h_5(k) &\triangleq \int_{a_0(k)}^{R} r\,C(r,k)\,\Phi(r;k)\,dr,\\
h_6(k) &\triangleq \int_{a_0(k)}^{R} r^2\,C(r,k)\,\Phi(r;k)\,dr.
\end{aligned}
\tag{12}
$$

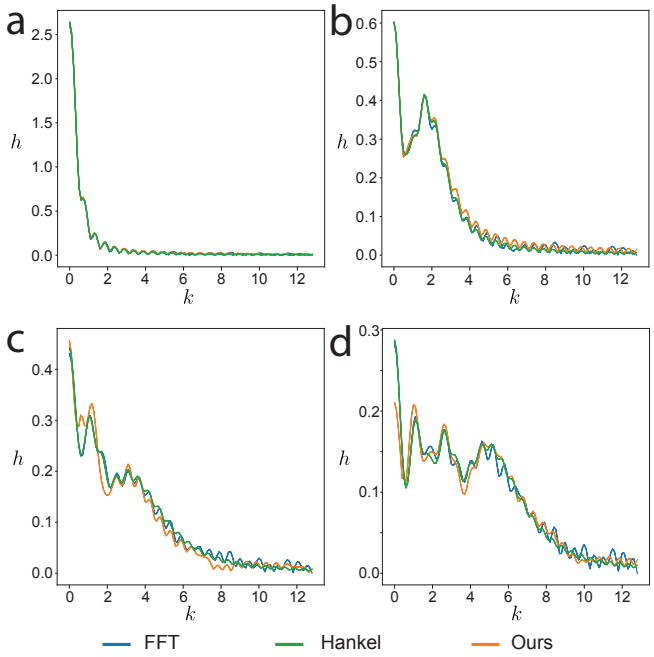

Fig. 4: Qualtitative comparison of radial PSF cross-sections using different simulators with sample defocus and spherical coefficients, C_d and C_s. (a) $C_d = 1, C_s = 0$. (b) $C_d = 5, C_s = 0$. (c) $C_d = 5, C_s = 5$. (d) $C_d = 10, C_s = 2$.

where

$$
\begin{aligned}
a_0(k) &\triangleq 1/(2\pi k),\\
\Phi(r) &\triangleq \exp\left(j\,2C_d r^2\right),\\
C(r,k) &\triangleq \cos\left(2\pi k r - \frac{\pi}{4}\right).
\end{aligned}
\tag{13}
$$

The weighted summation is:

$$
h(r) \approx 4\pi^2 \left| \sum_{i=1}^{6} c_i(k) h_i(k) \right|^2, \tag{14}
$$

where the coefficients are:

$$
c_1(k) = 1, \quad c_2(k) = -\pi^2 k^2, \quad c_3(k) = \frac{\pi^4 k^4}{4},
$$

$$
c_4(k) = \sqrt{\frac{2}{\pi}}\,\frac{1}{2\pi k}, \quad c_5(k) = \sqrt{\frac{2}{\pi}}\,\frac{3}{2}\alpha^{-1/2}, \quad c_6(k) = -\sqrt{\frac{2}{\pi}}\,\pi k\,\alpha^{-3/2}.
$$

The integrals h_{1-6} admit closed-form analytical solutions. For h_{1-3}, by applying the change of variables $u = r^2$, each integral reduces to the form $\int u^n e^{j(2C_d)u}\,du$, which can be evaluated in closed form using elementary functions. For h_{4-6}, the cosine modulation can be expressed as the sum of two complex exponentials: $C(r) = \frac{1}{2}\{e^{-j\pi/4}e^{j2\pi kr} + e^{j\pi/4}e^{-j2\pi kr}\}$. Each integral can then be written as the real part of an oscillatory integral of the form $\int r^m e^{j(\nu r^2+\gamma r)}\,dr$ with $\nu = 2C_d$ and $|\gamma| = 2\pi k$. Completing the square in the phase converts the $m = 0$ case into a complex Gaussian integral, yielding a closed-form expression in terms of the complex error function. The cases $m = 1$ and $m = 2$ follow from

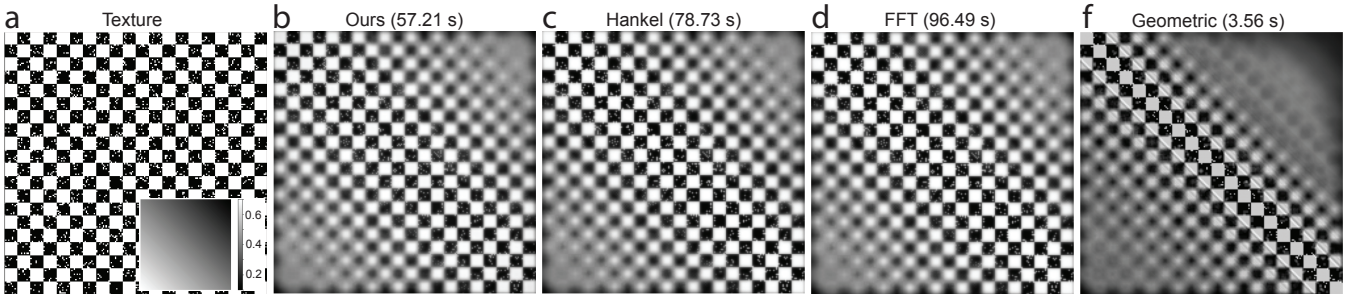

Fig. 5: Sample depth-of-field images rendered using different simulators. We calculate the PSF of each pixel according to the provided depth map (inset, unit: m) and sum the PSF weighted by the brightness of the pixel. The focal distance is $z_f = 0.4$ m, the sensor distance is $z_s = 12.37$ mm, the pupil radius is $R = 1$ mm, and the wavelength is $\lambda = 500$ nm. Ours achieves a clear speed advantage compared to Hankel and FFT. Although Geometric achieves the fastest rendering speed, it creates clear artifacts when the image is close to focus due to the discretization error of the scaling model.

algebraic recurrence identities that express higher-order moments in terms of the base integral and boundary exponential terms. The closed-form solutions are as follows. We omit the variable k for h_{1-6} and a_0 for simplicity.

$$
\begin{aligned}
h_1 &= \frac{e^{j2C_d a_0^2} - 1}{4jC_d}, \\
h_2 &= e^{j2C_d a_0^2}\left(\frac{a_0^2}{4jC_d} + \frac{1}{8C_d^2}\right) - \frac{1}{8C_d^2}, \\
h_3 &= e^{j2C_d a_0^2}\left(\frac{a_0^4}{4jC_d} + \frac{a_0^2}{4C_d^2} - \frac{1}{8jC_d^3}\right) + \frac{1}{8jC_d^3}, \\
h_4 &= \frac{e^{-j\pi/4}}{2}\Big(F_0(R,k) - F_0(a_0,k)\Big) \\
&\quad + \frac{e^{+j\pi/4}}{2}\Big(F_0(R,-k) - F_0(a_0,-k)\Big), \\
h_5 &= \frac{e^{-j\pi/4}}{2}\Big(F_1(R,k) - F_1(a_0,k)\Big) \\
&\quad + \frac{e^{+j\pi/4}}{2}\Big(F_1(R,-k) - F_1(a_0,-k)\Big), \\
h_6 &= \frac{e^{-j\pi/4}}{2}\Big(F_2(R,k) - F_2(a_0,k)\Big) \\
&\quad + \frac{e^{+j\pi/4}}{2}\Big(F_2(R,-k) - F_2(a_0,-k)\Big).
\end{aligned}
\tag{15}
$$

The intermediate elements F_{0-2} has the forms:

$$
\begin{aligned}
F_0(r,k) &= \mathcal{K}(r,k), \\
F_1(r,k) &= \frac{e^{j(2C_d r^2 + 2\pi k r)}}{4jC_d} - \frac{2\pi k}{4C_d}\,\mathcal{K}(r,k), \\
F_2(r,k) &= \frac{(4C_d r - 2\pi k)e^{j(2C_d r^2 + 2\pi k r)}}{16jC_d^2} \\
&\quad - \left(\frac{1}{4jC_d} - \frac{(2\pi k)^2}{16C_d^2}\right)\mathcal{K}(r,k),
\end{aligned}
\tag{16}
$$

where

$$
\mathcal{K}(r,k) \triangleq \exp\left(-j\frac{(2\pi k)^2}{8C_d}\right)\frac{\sqrt{\pi}}{2\sqrt{j\,2C_d}}\,\mathrm{erf}\left(j\sqrt{j\,2C_d}\left(r + \frac{2\pi k}{4C_d}\right)\right).
$$

6. REFERENCES

[1] Junjie Luo, Yuxuan Liu, Emma Alexander, and Qi Guo, "Depth from coupled optical differentiation: J. luo et al.," *International Journal of Computer Vision*, vol. 133, no. 11, pp. 8109–8126, 2025.

[2] Huixuan Tang, Scott Cohen, Brian Price, Stephen Schiller, and Kiriakos N Kutulakos, "Depth from defocus in the wild," in *Proceedings of the IEEE conference on computer vision and pattern recognition*, 2017, pp. 2740–2748.

[3] Yicheng Wu, Vivek Boominathan, Huaijin Chen, Aswin Sankaranarayanan, and Ashok Veeraraghavan, "Phasecam3d—learning phase masks for passive single view depth estimation," in *2019 IEEE International Conference on Computational Photography (ICCP)*. IEEE, 2019, pp. 1–12.

[4] Fu-Jen Tsai, Yan-Tsung Peng, Yen-Yu Lin, Chung-Chi Tsai, and Chia-Wen Lin, "Stripformer: Strip transformer for fast image deblurring," in *European conference on computer vision*. Springer, 2022, pp. 146–162.

[5] Lingshun Kong, Jiangxin Dong, Jianjun Ge, Mingqiang Li, and Jinshan Pan, "Efficient frequency domain-based transformers for high-quality image deblurring," in *Proceedings of the IEEE/CVF Conference on Computer Vision and Pattern Recognition*, 2023, pp. 5886–5895.

[6] Chrispin Jiji, VL Nandhini, VL Malini, and R Ciro Rodriguez, "Extended depth of focus imaging using optics and image processing," *International Journal of Information Technology*, vol. 16, no. 2, pp. 1137–1143, 2024.

[7] Brian A Barsky and Todd J Kosloff, "Algorithms for rendering depth of field effects in computer graphics,"

in *Proceedings of the 12th WSEAS international conference on Computers*. World Scientific and Engineering Academy and Society (WSEAS), 2008, vol. 2008.

[8] Jaroslav Křivánek, Jiri Zara, and Kadi Bouatouch, "Fast depth of field rendering with surface splatting," in *Proceedings Computer Graphics International 2003*. IEEE, 2003, pp. 196–201.

[9] Dean S Hazineh, Soon Wei Daniel Lim, Zhujun Shi, Federico Capasso, Todd Zickler, and Qi Guo, "D-flat: A differentiable flat-optics framework for end-to-end metasurface visual sensor design," *arXiv preprint arXiv:2207.14780*, 2022.

[10] Johannes E Fröch, Praneeth Chakravarthula, Jipeng Sun, Ethan Tseng, Shane Colburn, Alan Zhan, Forrest Miller, Anna Wirth-Singh, Quentin AA Tanguy, Zheyi Han, et al., "Beating spectral bandwidth limits for large aperture broadband nano-optics," *Nature communications*, vol. 16, no. 1, pp. 3025, 2025.

[11] Ethan Tseng, Shane Colburn, James Whitehead, Luocheng Huang, Seung-Hwan Baek, Arka Majumdar, and Felix Heide, "Neural nano-optics for high-quality thin lens imaging," *Nature communications*, vol. 12, no. 1, pp. 6493, 2021.

[12] Stanley H Chan, Nicholas Chimitt, et al., "Computational imaging through atmospheric turbulence," *Foundations and Trends® in Computer Graphics and Vision*, vol. 15, no. 4, pp. 253–508, 2023.

[13] J. Goodman, *Fourier Optics*, McGraw-Hill, New York, 2 edition, 1996.

[14] Chi-Jui Ho, Yash Belhe, Steve Rotenberg, Ravi Ramamoorthi, Tzu-Mao Li, and Nicholas Antipa, "A differentiable wave optics model for end-to-end computational imaging system optimization," in *Proceedings of the IEEE/CVF International Conference on Computer Vision*, 2025, pp. 28042–28051.

[15] Zheng Ren, Jingwen Zhou, Wenguan Zhang, Jiapu Yan, Bingkun Chen, Huajun Feng, and Shiqi Chen, "Successive optimization of optics and post-processing with differentiable coherent psf operator and field information," *IEEE Transactions on Computational Imaging*, 2025.

[16] Ethan Tseng, Ali Mosleh, Fahim Mannan, Karl St-Arnaud, Avinash Sharma, Yifan Peng, Alexander Braun, Derek Nowrouzezahrai, Jean-Francois Lalonde, and Felix Heide, "Differentiable compound optics and processing pipeline optimization for end-to-end camera design," *ACM Transactions on Graphics (TOG)*, vol. 40, no. 2, pp. 1–19, 2021.

[17] Esther YH Lin, Zhecheng Wang, Rebecca Lin, Daniel Miau, Florian Kainz, Jiawen Chen, Xuaner Zhang, David B Lindell, and Kiriakos N Kutulakos, "Learning lens blur fields," *IEEE Transactions on Pattern Analysis and Machine Intelligence*, 2025.

[18] Zhiyuan Mao, Nicholas Chimitt, and Stanley H Chan, "Accelerating atmospheric turbulence simulation via learned phase-to-space transform," in *Proceedings of the IEEE/CVF international conference on computer vision*, 2021, pp. 14759–14768.

[19] AJS Hamilton, "Uncorrelated modes of the non-linear power spectrum," *Monthly Notices of the Royal Astronomical Society*, vol. 312, no. 2, pp. 257–284, 2000.

[20] M. Abramowitz and I. A. Stegun, *Handbook of Mathematical Functions with Formulas, Graphs, and Mathematical Tables*, U.S. Dept. of Commerce, 9 edition, 1964.

[21] James C Wyant and Katherine Creath, "Basic wavefront aberration theory for optical metrology," *Applied optics and optical engineering*, vol. 11, no. part 2, pp. 28–39, 1992.